Title

In vitro and ex vivo characterization of (−)-TZ659 as a ligand for imaging the vesicular acetylcholine transporter

Authors

Liu, Hui
Jin, Hongjun
Li, Junfeng
et al.

Publication Date

2015-04-01

DOI

10.1016/j.ejphar.2015.02.001

Peer reviewed

HHS Public Access

Author manuscript

Eur J Pharmacol. Author manuscript; available in PMC 2016 April 05.

Published in final edited form as:

Eur J Pharmacol. 2015 April 5; 752: 18–25. doi:10.1016/j.ejphar.2015.02.001.

In vitro and *ex vivo* characterization of (-)-TZ659 as a ligand for imaging the vesicular acetylcholine transporter

Hui Liu[1], **Hongjun Jin**[1], **Junfeng Li**[1], **Xiang Zhang**[1], **Kota Kaneshige**[2], **Stanley M. Parsons**[2], **Joel S. Perlmutter**[1,3], and **Zhude Tu**[1,*]

[1]Department of Radiology, Washington University School of Medicine, St. Louis, MO 63110, USA

[2]Department of Chemistry and Biochemistry, University of California, Santa Barbara, CA 93106, USA

[3]Department of Neurology, Washington University School of Medicine, St. Louis, MO 63110, USA

Abstract

The loss of cholinergic neurons and synapses relates to the severity of dementia in several neurodegenerative pathologies; and the vesicular acetylcholine transporter (VAChT) provides a reliable biomarker of cholinergic function. We recently characterized and ^{11}C-labeled a new VAChT inhibitor, (-)-**TZ659**. Here we report the *in vitro* and *ex vivo* characterization of (-)-**TZ659**. A stably transfected PC12$^{A123.7}$ cell line which expresses human VAChT (hVAChT) was used for the *in vitro* binding characterization of (-)-[^{3}H]**TZ659.** A saturated binding curve was obtained with K_d = 1.97 ± 0.30 nM and B_{max} = 3240 ± 145.9 fmol/mg protein. In comparison, a PC12$^{A123.7}$ cell line that expresses mutant hVAChT showed decreased binding affinity (K_d = 15.94 ± 0.28 nM). Competitive binding assays using a panel of other CNS ligands showed no inhibition of (-)-[^{3}H]**TZ659** binding. On the other hand, binding inhibitions were observed only using VAChT inhibitors (K_i = 0.20 nM - 31.35 nM). An *in vitro* assay using rat brain homogenates showed that (-)-[^{3}H]**TZ659** had higher binding in striatum than in cerebellum, with a target: non-target ratio > 3.46. Even higher *ex vivo* striatum-to-cerebellum ratios (9.56 ± 1.11) were observed using filtered homogenates of brain tissue after rats were injected intravenously with (-)-[^{11}C]**TZ659**. *Ex vivo* autoradiography of (-)-[^{11}C]**TZ659** confirmed high striatal uptake, with a consistently high striatum-to-cerebellum ratio (2.99 ± 0.44). In conclusion, (-)-**TZ659** demonstrated high potency and good specificity for VAChT *in vitro* and *in vivo*. These data suggest that (-)-[^{11}C]**TZ659** may be a promising PET tracer to image VAChT in the brain.

Keywords

vesicular acetylcholine transporter; radioligand; binding assay; autoradiography

*Corresponding author. Tel.: +1-314-362-8487; Fax: +1-314-362-8555; tuz@mir.wustl.edu.

Disclosure: The authors do not have any conflict of interest.

1. Introduction

Loss of cholinergic neurons/terminals in the brain strongly correlates with cognitive impairment in patients with dementia (Armstrong, 2013; Davies and Maloney, 1976; Schliebs and Arendt, 2011). Postmortem and neuroimaging studies in patients with Parkinson's disease dementia (PDD) reveal a similar relationship between cholinergic function and cognitive performance (Bohnen and Albin, 2011; Pavese, 2012). Moreover, cholinergic degeneration in Parkinson's disease (PD) likely begins prior to dementia (Shimada et al., 2009). These findings highlight the importance of cholinergic dysfunction which extend to acetylcholine-dopamine interactions in the striatum (Bohnen and Albin, 2011; Lester et al., 2010). Therefore, *in vivo* measurement of cholinergic dysfunction may provide a critical biomarker for understanding pathophysiology and treatment of these diseases.

Positron emission tomography (PET) imaging is a non-invasive modality that can assess the density of neuronal biomarkers in the central nervous system (CNS), and thus provide neurological information regarding molecular and cellular function in living subjects. Tremendous efforts have been put forth towards the identification of a PET tracer suitable for evaluating cholinergic function in the human brain. PET imaging of acetylcholinesterase (AChE) is one strategy that has been successfully used to study patients with dementia (Kikuchi et al., 2013). Unfortunately, AChE enzyme activity may not functionally correlate with loss of cholinergic terminals. Another reliable marker of cholinergic neurons, choline acetyltransferase (ChAT), has not been imaged successfully *in vivo*. Vesicular acetylcholine transporter (VAChT), which loads acetylcholine into presynaptic vesicles, maps to cholinergic cells in the brain and displays a good correspondence with ChAT (Weihe et al., 1996). A PET tracer for VAChT could thus be used to assess cholinergic function in human subjects and monitor the therapeutic efficacy of VAChT inhibition strategies.

A number of radiolabeled benzovesamicol analogues have been evaluated as VAChT imaging agents (Giboureau et al., 2010). However, when tested in pre-clinical studies and human subjects, most of these radiotracers showed poor selectivity over σ receptors in brain, low extraction from the blood, slow brain kinetics, or rapid metabolism (Li et al., 2013). Despite a slow brain kinetic, [^{18}F]FEOBV is the only PET tracer approved for imaging VAChT in human brains (Giboureau et al., 2007; Kilbourn et al., 2009; Petrou et al., 2014). Recently, our group designed a new class of VAChT inhibitors including (-)-**TZ659**, which contain a carbonyl group attached to the 4-position of the piperidine ring (Efange et al., 2010; Li et al., 2013; Tu et al., 2009; Tu et al., 2012). (-)-**TZ659** has a high affinity for VAChT, and a high selectivity for VAChT over σ_1 and σ_2 receptors; (-)-[^{11}C]**TZ659** was successfully radiolabeled and showed a higher accumulation in the striatum of rats and nonhuman primates than in other non-target brain regions (Li et al., 2013). Here we further reported the *in vitro* and *ex vivo* pharmacology of (-)-[^{11}C]**TZ659** and its tritiated counterpart, (-)-[^{3}H]**TZ659**. (-)-**TZ659** binds to VAChT with a high potency and good specificity for VAChT versus other CNS targets. Both (-)-[^{11}C]**TZ659** and (-)-[^{3}H]**TZ659** showed higher uptake in the VAChT-enriched striatum than the reference brain region (cerebellum).

2. Materials and Methods

2.1 Radioligand preparation

The two-step synthesis of (-)-[^{11}C]**TZ659** was carried out as previously reported (Li et al., 2013). The tritiated compound (-)-[^{3}H]**TZ659** was custom synthesized by American Radiolabeled Chemicals, Inc. (St. Louis, MO) using the Boc-protected amino precursor and the synthetic strategy employed for ^{11}C-labeling.

2.2 Drugs and preparation of stock solutions

Reagents and standard compounds for *in vitro* assays were purchased from Sigma (St. Louis, MO) and Tocris Biosciences (R&D Systems, Minneapolis, MN) unless otherwise noted. Novel compounds were synthesized in-house. Test compounds (structures are shown in Fig. 1) were dissolved in *N*,*N*-dimethylformamide or ethanol to create a stock solution; the desired concentration for *in vitro* assays was subsequently obtained by further dilution in the assay buffer (50 mM Tris-HCl, 120 mM NaCl, 5 mM KCl, 2 mM $CaCl_2$, 1 mM $MgCl_2$, pH 7.4).

2.3 Radioligand binding assays in cell post-nuclear supernatant

2.3.1 Cell culture—PC12$^{A123.7}$ cells stably transfected with human VAChT (hVAChT) wild type (GenBank: AAA20497.1) or W331A mutant cDNA were grown at 37 °C in 5% CO_2 in complete Dulbecco's modified Eagle's medium mixed 1: 1 with Ham's F-12 medium. The complete medium was supplemented with 10% horse serum, 5% fetal bovine serum, 100 units penicillin/ml, 100 μg streptomycin/ml, and 10 μg blasticidin/ml. Site-directed mutagenesis of W331 previously identified the W331A mutation which exhibits non-specific vesamicol binding but no transport of ACh. Stable transfection of cells with W331A was performed as previously reported (Khare et al., 2010). PC12$^{A123.7}$ cells transfected with the blank parent vector served as the background control.

2.3.2 Preparation of post-nuclear supernatants from transfected cells—Cells were harvested, resuspended in cold (4 °C) homogenization buffer (0.32 M sucrose, 4 mM HEPES-NaOH, 1 mM EDTA, pH 7.4), and gently homogenized. The suspension was centrifuged at 800 ×*g* for 10 min to pellet debris, then the post-nuclear supernatant was centrifuged at 18000 ×*g* for 30 min. The pellet was suspended in the assay buffer and was stored at -80 °C until use. The protein concentration of the suspension was determined using the Detergent Compatible (DC) protein assay (Bio-Rad, Hercules, CA) following the manufacturer's instructions.

2.3.3 Saturation binding assay—Post-nuclear supernatants were diluted and incubated for 60 min with (-)-[^{3}H]**TZ659** in a total volume of 150 μl at 25 °C in 96-well polypropylene plates (Fisher Scientific, Pittsburgh, PA). Each well contained 20 μg protein while the concentration of the radioligand ranged from 0.15 nM to 20 nM. Reactions were terminated by the addition of 100 μl of the assay buffer at 4 °C, then samples were harvested and filtered rapidly using a 96-well glass fiber filtration plate (Millipore, Billerica, MA) presoaked with 100 μl assay buffer for 1 hour. Each filter was washed with 5 × 200 μl assay buffer then transferred to a scintillation vial with 2 ml of scintillation fluid and counted on a

Wallac 1450 MicroBeta TriLux liquid scintillation counter (Perkin Elmer, Boston, MA). Nonspecific binding was determined from samples which contained 20 μM (-)-vesamicol hydrochloride. Counts were normalized to mg protein in the sample. The equilibrium dissociation constant (K_d) and maximum number of binding sites (B_{max}) were determined by nonlinear regression analysis of onesite saturation binding model using GraphPad Prism 5.0 (GraphPad Software, Inc., San Diego, CA). Three independent experiments were performed; the results are reported as mean ± standard deviation.

2.3.4 Competitive binding assay—A panel of ligands for CNS targets including VAChT, σ_1 receptor, σ_2 receptor, dopamine D_2 receptor, vesicular monoamine transporter 2 (VMAT2), serotonin 1A ($5\text{-}HT_{1A}$) receptor, and phosphodiesterase 10A (PDE10A) was used to characterize the pharmacological profile of (-)-[^{3}H]**TZ659** via a competitive binding assay. Post-nuclear supernatants (20 μg protein) were diluted with the assay buffer and incubated with each test ligand in a total volume of 150 μl with (-)-[^{3}H]**TZ659** in 96 well plates for 60 min at 25 °C. The final concentration of the radioligand in each assay was 2 nM. Concentrations of test ligands ranged from 0.1 nM to 10 μM and were used to determine K_i values for each compound. After incubation, the samples were washed 5 times and the bound radioactivity counted and analyzed by nonlinear regression using one-site competitive binding model using GraphPad Prism 5.0 (GraphPad Software, Inc., San Diego, CA). Nonspecific binding was determined from samples that contained 20 μM of (-)-vesamicol hydrochloride. Three independent experiments were performed; the results are reported as mean ± standard deviation.

2.4 *In vitro* and *ex vivo* rodent studies

All animal experiments were conducted in compliance with the Guidelines for the Care and Use of Research Animals under protocols approved by Washington University's Animal Studies Committee. Mature, male Sprague–Dawley (SD) rats (Charles River Laboratories, Inc., Wilmington, MA) were used for all experiments. Tail vein injections were performed under light inhalation anesthesia (1-2% isoflurane/oxygen) and euthanasia was done under surgical plane anesthesia.

2.4.1 *In vitro* binding assay in rat brain homogenates—Male SD rats weighing 250-300 g were euthanized as described above and the whole brain was immediately removed. Excess blood was blotted from the tissue; striatum and cerebellum were collected and homogenized in cold (4 °C) homogenization buffer (0.32 M sucrose, 4 mM HEPES-NaOH, 1 mM EDTA, pH 7.4); 1.5-2.0 ml buffer was added per 100 mg tissue. An aliquot of homogenate was used to measure protein content by the DC protein assay as previously described. The crude homogenates of striatum and cerebellum were diluted for the *in vitro* binding assay and incubated for 60 min with (-)-[^{3}H]**TZ659** in a total volume of 150 μl at 25 °C as described above. The concentration of the radioligand ranged from 0.65 nM to 5.21 nM. After the incubation, the samples were washed and the bound radioactivity counted as described above. Two or three independent experiments were performed.

2.4.2 *Ex vivo* uptake ratio for rat striatum to cerebellum—The *ex vivo* striatum to cerebellum uptake ratio of (-)-[^{11}C]**TZ659** was determined using tissue homogenates as

previously described by Larsen *et al.* (Larsen et al., 2004). This approach was recently used by Kehler *et al.* prior to conducting *ex vivo* binding assays of a ^{11}C-labeled PDE10A tracer (Kehler et al., 2014). Adult male SD rats (250 - 300 g, n = 4) were anesthetized and injected with 3.0-3.5 mCi (-)-[^{11}C]**TZ659**. Rats were euthanized 60 min after injection, and the whole brain was immediately removed. Excess blood was blotted from the tissue and striatum and cerebellum were collected. The tissues were homogenized in ice-cold assay buffer. 1.5-2.0 ml buffer was added per 100 mg tissue. An aliquot of homogenate was used to measure protein content by the DC protein assay as previously described. 300 μl of striatal or cerebellar homogenate was added to each well (samples were run for n = 4 rats) and immediately filtered through 96-well glass fiber filtration plates. The filters were washed twice and the bound radioactivity counted as described above.

2.5 *Ex vivo* autoradiography in rats

Adult male SD rats (250-300 g, n = 3) were injected with 4.0 - 4.5 mCi (-)-[^{11}C]**TZ659**. Rats were euthanized 60 min after injection, and the whole brain was immediately removed. Intact brains were snap frozen over dry ice. Horizontal sections (100 μm) were cut with a Microm cryotome and mounted on Superfrost Plus glass slides (Fisher Scientific, Pittsburgh, PA). Frozen slides were directly exposed to film in an imaging cassette BAS-TR2025 (Fuji Photo Film Co., Tokyo, Japan) for 12 hours at -80 °C in the dark. The distribution of radioactivity was visualized by a Fuji Bio-Imaging Analyzer FLA-7000 (Fuji Photo Film Co., Tokyo, Japan). Photo-stimulated luminescence (PSL) from the striatum and cerebellum was quantified using Multi Gauge v3.0 software (Fuji Photo Film Co., Tokyo, Japan). Data were background-corrected and expressed as photo-stimulated luminescence signals per square millimeter (PSL/mm^2).

2.6 Homology docking of hVAChT

The interactions of the hVAChT and the ligand (-)-**TZ659** were evaluated using protein docking by polar Fourier correlations (http://hexserver.loria.fr) (Ritchie and Venkatraman, 2010). Molecular interaction analysis was performed using UCSF Chimera analysis (Pettersen et al., 2004). The major facilitator superfamily (MFS) homology structure of hVAChT was produced by Dr. Lucy R. Forrest (Radestock and Forrest, 2011). The 3D structure of (-)-**TZ659** was created using ChemBioDraw 13.0 (CambridgeSoft Software, PerkinElmer Inc. Waltham, MA). Total energy of interactions were calculated based on shape and electrostatics as correlation type and the final search was set to 15 (N = 15); the angular search range of docking parameters were set to default values. The best docking structure of complex for hVAChT and (-)-**TZ659**, which showed the lowest energy from the 15 solutions, was subjected to further molecular interaction studies.

3. Results

3.1 Radiolabeling

The chemical structure of (-)-[^{3}H]**TZ659** and (-)-[^{11}C]**TZ659** are shown in Fig. 1. The specific activity of (-)-[^{3}H]**TZ659** was 80 Ci/mmol. (-)-[^{11}C]**TZ659** was obtained in high radiochemical yield (55-70%, decay corrected), with radiochemical purity > 98% and

specific activity >4,000 Ci/mmol (decay corrected to end of bombardment). The synthesis of (-)-[^{11}C]**TZ659** was accomplished as reported previously (Li et al., 2013).

3.2 *In vitro* radioligand binding assay using post-nuclear supernatants of PC12$^{A123.7}$ cells

Initial saturation binding studies were carried out using (-)-[^{3}H]**TZ659** with post-nuclear supernatants of transfected PC12$^{A123.7}$ cells which express wild type W331 hVAChT. A saturation binding curve revealed K_d = 1.97 ± 0.30 nM and B_{max} = 3240.00 ± 145.90 fmol/mg protein (Fig. 2A). Post-nuclear supernatants of PC12$^{A123.7}$ cells stably transfected with mutant W331A hVAChT also showed saturation binding, with a higher K_d (15.94 ± 1.35 nM) and a lower B_{max} (2605 ± 115.90 fmol/mg protein) (Fig. 2B). In the background control assay using a blank transfection vector, no saturation curve could be obtained, and the measured radioactivity was much lower than that of the nonspecific binding. These results suggested that the binding of (-)-[^{3}H]**TZ659** to post-nuclear supernatants of PC12$^{A123.7}$ cells is specifically due to the hVAChT protein.

The competitive binding assays showed that VAChT inhibitors (-)-TZ2144, TZ4376, FBBV and (-)-vesamicol displaced (-)-[^{3}H]**TZ659** binding with K_i values of 0.20 nM, 1.82 nM, 7.17 nM and 31.35 nM, respectively (Fig. 2C). VAChT ligands TZ4376 and FBBV were previously reported by our group (Li et al., 2013; Tu et al., 2009). (-)-TZ2144 is a new compound synthesized in our lab; its synthesis will be reported elsewhere. No inhibition of (-)-[^{3}H]**TZ659** binding to VAChT was observed in the competitive binding studies using other CNS receptor ligands: (+)-pentazocine (σ_1 receptor, (Steinfels et al., 1988)), ISO-1 (σ_2 receptor, (Tu et al., 2007)), *S*-(-)-eticlopride (dopamine D_2 receptor, (Kohler et al., 1985)), DTBZ (VMAT2, (Kilbourn et al., 1995)), WAY-100135 (5-HT_{1A} receptor, (Fletcher et al., 1993)), and MP-10 (PDE10A, (Verhoest et al., 2009)). The K_i values are summarized in Table 1. The data indicates that (-)-[^{3}H]**TZ659** binds to VAChT with high selectivity.

3.3 *In vitro* and *ex vivo* assays using rat brain homogenates

The *in vitro* binding assay using (-)-[^{3}H]**TZ659** and rat brain homogenates, showed higher total binding levels in the striatum and lower levels in the cerebellum, demonstrating a high target: nontarget ratio at various tracer concentrations (ratio > 3.46; Fig. 3A). Prior studies of the time-dependent regional brain distribution of (-)-[^{11}C]**TZ659** in rats (data not shown) led to selection of 60 min post injection for the uptake study. After tissue homogenization and filtration, a higher striatum: cerebellum ratio was observed (9.56 ± 1.11; Fig. 3B), compared with the *in vitro* binding study.

3.4 Autoradiography using rat brains

Ex vivo autoradiography studies were performed to confirm the regional selectivity of radiolabeled (-)-**TZ659** in the rat brain. (-)-[^{11}C]**TZ659** clearly accumulated in the VAChT-enriched striatum with little accumulation in the cerebellum (Fig. 4). The uptake of (-)-[^{11}C]**TZ659** in rat striatum was 2.99-fold higher than that in cerebellum.

3.5 Homology docking of hVAChT

The molecular docking using the HEX server acquired 15 docking complex structures for hVAChT and (-)-**TZ659**. The most representative (as shown in Fig. 5A) of the 15 solutions, with lowest docked energy (E_{total} = -293.36 kcal/mol), was chosen for further analysis. Our docking results indicated that (-)-**TZ659** binds to hVAChT at the conserved MFS pocket near Tyr50, Glu309, Trp331 (W331) and Tyr 428 (Fig. 5B).

4. Discussion

Although different strategies can be used to assess the integrity of the cholinergic system in the CNS, interpreting results from imaging studies using AChE ligands can be challenging (Nagren et al., 2010). VAChT provides a pre-synaptic target localized to cholinergic terminals (Gilmor et al., 1996), thus VAChT imaging should directly reflect changes in the density of cholinergic terminals. An additional potential clinical advantage of a VAChT radioligand is that it may allow *in vivo* assessment of the integrity of cholinergic nerve terminals in patients taking cholinesterase inhibitor drugs (Bohnen and Albin, 2011). Radiolabeled benzovesamicol analogues have been used to measure VAChT density as a biomarker of neurodegenerative diseases for almost two decades (Kuhl et al., 1996; Mulholland et al., 1998; Parent et al., 2013; Petrou et al., 2014; Pirker et al., 2003; Seibyl et al., 1995). Neuroimaging findings using SPECT and PET ligands are consistent with postmortem evidence indicating that basal forebrain cholinergic deficits appear early in PD (Ruberg et al., 1986). A recent microPET study using (-)-[^{18}F]FEOBV in a rat model of cholinergic denervation detected neuronal terminal losses induced by selective lesions of the pedunculopontine (PPTg) nucleus; the imaging results were confirmed by ChAT immunostaining (Cyr et al., 2014).

Our group previously reported the synthesis and the preliminary evaluation of (-)-**TZ659**. Competitive radioligand binding assays revealed that (-)-**TZ659** possesses a high VAChT potency with a K_i value of 0.78 nM determined using (-)-[^{3}H]vesamicol, and poor affinities for both σ_1 receptors (K_i = 992 nM, determined using (+)- [^{3}H]pentazocine, and σ_2 receptors (K_i = 11,400 nM, determined using [^{3}H]DTG); the selectivity of (-)**TZ659** binding toward VAChT over $\sigma_1$and σ_2 receptors is over 1200-fold (Li et al., 2013). Biodistribution studies in rats and microPET studies in nonhuman primates showed good accumulation in the VAChT enriched striatal regions (Li et al., 2013). Here we extend these studies and provide *in vitro* and *ex vivo* characterization of tritiated (-)-**TZ659** for *in vitro* assays. Saturation binding assays of (-)-[^{3}H]**TZ659** in homogenates of PC12$^{A123.7}$ cells transfected with wild-type W331 hVAChT cDNA were performed using (-)-vesamicol to define non-specific binding. It was found that (-)-[^{3}H]**TZ659** had a single high affinity binding site. The K_d value of (-)-[^{3}H]**TZ659** (1.97 nM) is close to the previously reported K_i value (0.78 nM) of (-)-**TZ659** for VAChT (Li et al., 2013). When using the PC12$^{A123.7}$ cells transfected with blank vector as a background control, the readouts of total binding and non-specific binding were too close to determine a real saturated binding status, which indicates that PC12 cells which are not transfected with hVAChT contain very few (-)-[^{3}H]**TZ659** binding sites. In addition, PC12$^{A123.7}$ cells were stably transfected with mutant W331A hVAChT, as reported in previous docking and mutagenesis studies of hVAChT (Khare et al., 2010). Site-

directed mutagenesis of W331 in the lumenal beginning of transmembrane helix VI of VAChT by Khare *et al*. identified the region as critical for specific binding. Cells transfected with W331A mutant hVAChT exhibit non-specific vesamicol binding but no transport of ACh (Khare et al., 2010). The W331A mutation decreased binding affinity of the tracer by ∼8 fold (the K_i value changed from 1.97 nM to 15.94 nM), which further supports the binding specificity of (-)-[^{3}H]**TZ659** for VAChT. In line with this finding, our docking calculations suggest that the residue W331 may interact by hydrophobic stacking with the aromatic ring of (-)-**TZ659**; formation of hydrogen bonds suggests potential interactions between Glu309 and the carbonate group, which might contribute to the high selectivity of (-)-**TZ659** for VAChT compared with other vesamicol analogues (Li et al., 2013; Tu et al., 2009).

Using the homogenates of PC12$^{A123.7}$ cells transfected with wild-type hVAChT cDNA, the competitive binding assay confirmed that (-)-[^{3}H]**TZ659** has little affinity for σ_1, σ_2, VMAT2, dopaminergic, serotonergic, or PDE10A receptors/proteins. This finding is in agreement with the $K_{i\text{-non-target}}$/ $K_{i\text{-VAChT}}$ ratios of the corresponding cold compound (over 1200- fold selectivity) (Li et al., 2013). Moreover, the low K_i values calculated from competitive binding assays using VAChT inhibitors, the carbonyl group-containing analogues (-)-TZ2144, TZ4376, FBBV and (-)-vesamicol, suggest those ligands have the same binding site as (-)-[^{3}H]**TZ659**, which is also one of the carbonyl group-containing analogues. Together, these results indicate that the binding of (-)-[^{3}H]**TZ659** is specific for VAChT.

We further investigated the selectivity of radiolabeled (-)-**TZ659** for striatal tissue in rats using three different methods, including *in vitro* binding assays using (-)-[^{3}H]**TZ659**, *ex vivo* uptake assays using (-)-[^{11}C]**TZ659**, and *ex vivo* autoradiography using (-)-[^{11}C]**TZ659**. Immunostaining of rat brain for VAChT (Gilmor et al., 1996) and preclinical imaging studies of VAChT (Efange, 2000) both indicate that the striatum is the target region for VAChT, with the cerebellum as an appropriate reference region. Both of our *in vitro* binding assays using (-)-[^{3}H]**TZ659** and *ex vivo* uptake assays using (-)-[^{11}C]**TZ659** showed a significant accumulation of the radioactivity in the striatum compared with the cerebellum; this is in agreement with the reported distribution of VAChT in the brain (Gilmor et al., 1996). Interestingly, although the target: non-target ratio for (-)-[^{11}C]**TZ659** in *ex vivo* autoradiography was lower than results from the other two methods, the ratio was closer to the result from PET imaging studies in nonhuman primates (Li et al., 2013). Despite differences in the absolute values obtained, all three measurements consistently revealed that radiolabeled (-)-**TZ659** are highly accumulated in the striatum.

In conclusion, this work demonstrates that (-)-[^{11}C]**TZ659**, which has high affinity and specificity to VAChT, has high potential to be a suitable PET tracer for assessing the level of VAChT in the brain. Further work is needed to determine the pharmacokinetics of (-)-[^{11}C]**TZ659** *in vivo*, and to evaluate the utility of this new PET radiotracer using animal models of cholinergic denervation.

Acknowledgments

This work was supported by the National Institute of Neurological Disorders and Stroke (NINDS, No. R01NS075527, RO1NS058714), National Institute of Mental Health (NIMH) of the National Institutes of Health (No. MH092797), the American Parkinson Disease Association (APDA), the Greater St. Louis Chapter of the APDA and Barnes-Jewish Hospital Foundation (the Elliot Stein Family Endowment and the Parkinson Disease Research Fund). The authors thank. Lynne Jones and Adam Rosenberg for manuscript revision, and Jinbin Xu for technical assistance with the binding assays.

References

Armstrong RA. What causes Alzheimer's disease? Folia neuropathologica / Association of Polish Neuropathologists and Medical Research Centre. Polish Academy of Sciences. 2013; 51:169–188.

Bohnen NI, Albin RL. The cholinergic system and Parkinson disease. Behavioural brain research. 2011; 221:564–573. [PubMed: 20060022]

Cyr M, Parent MJ, Mechawar N, Rosa-Neto P, Soucy JP, Aliaga A, Kostikov A, Maclaren DA, Clark SD, Bedard MA. PET imaging with [^{18}F]fluoroethoxybenzovesamicol ([^{18}F]FEOBV) following selective lesion of cholinergic pedunculopontine tegmental neurons in rat. Nucl Med Biol. 2014; 41:96–101. [PubMed: 24267056]

Davies P, Maloney AJ. Selective loss of central cholinergic neurons in Alzheimer's disease. Lancet. 1976; 2:1403. [PubMed: 63862]

Efange SM. In vivo imaging of the vesicular acetylcholine transporter and the vesicular monoamine transporter. FASEB journal : official publication of the Federation of American Societies for Experimental Biology. 2000; 14:2401–2413. [PubMed: 11099458]

Efange SM, Khare AB, von Hohenberg K, Mach RH, Parsons SM, Tu Z. Synthesis and in vitro biological evaluation of carbonyl group-containing inhibitors of vesicular acetylcholine transporter. Journal of medicinal chemistry. 2010; 53:2825–2835. [PubMed: 20218624]

Fletcher A, Bill DJ, Bill SJ, Cliffe IA, Dover GM, Forster EA, Haskins JT, Jones D, Mansell HL, Reilly Y. WAY100135: a novel, selective antagonist at presynaptic and postsynaptic 5-HT$_{1A}$ receptors. Eur J Pharmacol. 1993; 237:283–291. [PubMed: 8365456]

Giboureau N, Emond P, Fulton RR, Henderson DJ, Chalon S, Garreau L, Roselt P, Eberl S, Mavel S, Bodard S, Fulham MJ, Guilloteau D, Kassiou M. Ex vivo and in vivo evaluation of (2*R*,3*R*)-5-[^{18}F]-fluoroethoxy- and fluoropropoxy-benzovesamicol, as PET radioligands for the vesicular acetylcholine transporter. Synapse (New York, NY). 2007; 61:962–970.

Giboureau N, Som IM, Boucher-Arnold A, Guilloteau D, Kassiou M. PET radioligands for the vesicular acetylcholine transporter (VAChT). Current topics in medicinal chemistry. 2010; 10:1569–1583. [PubMed: 20583990]

Gilmor ML, Nash NR, Roghani A, Edwards RH, Yi H, Hersch SM, Levey AI. Expression of the putative vesicular acetylcholine transporter in rat brain and localization in cholinergic synaptic vesicles. The Journal of neuroscience : the official journal of the Society for Neuroscience. 1996; 16:2179–2190. [PubMed: 8601799]

Kehler J, Kilburn JP, Estrada S, Christensen SR, Wall A, Thibblin A, Lubberink M, Bundgaard C, Brennum LT, Steiniger-Brach B, Christoffersen CT, Timmermann S, Kreilgaard M, Antoni G, Bang-Andersen B, Nielsen J. Discovery and development of ^{11}C-Lu AE92686 as a radioligand for PET imaging of phosphodiesterase 10A in the brain. Journal of Nuclear Medicine. 2014; 55:1513–1518. [PubMed: 24994928]

Khare P, Mulakaluri A, Parsons SM. Search for the acetylcholine and vesamicol binding sites in vesicular acetylcholine transporter: The region around the lumenal end of the transport channel. Journal of neurochemistry. 2010; 115:984–993. [PubMed: 20831599]

Kikuchi T, Okamura T, Zhang MR, Irie T. PET probes for imaging brain acetylcholinesterase. Journal of labelled compounds & radiopharmaceuticals. 2013; 56:172–179. [PubMed: 24285323]

Kilbourn M, Lee L, Vanderborght T, Jewett D, Frey K. Binding of Alpha-Dihydrotetrabenazine to the Vesicular Monoamine Transporter Is Stereospecific. Eur J Pharmacol. 1995; 278:249–252. [PubMed: 7589162]

Kilbourn MR, Hockley B, Lee L, Sherman P, Quesada C, Frey KA, Koeppe RA. Positron emission tomography imaging of (*2R,3R*)-5-[^{18}F]fluoroethoxybenzovesamicol in rat and monkey brain: a radioligand for the vesicular acetylcholine transporter. Nuclear medicine and biology. 2009; 36:489–493. [PubMed: 19520289]

Kohler C, Hall H, Ogren SO, Gawell L. Specific in vitro and in vivo binding of 3H-raclopride. A potent substituted benzamide drug with high affinity for dopamine D-2 receptors in the rat brain. Biochemical pharmacology. 1985; 34:2251–2259. [PubMed: 4015674]

Kuhl DE, Minoshima S, Fessler JA, Frey KA, Foster NL, Ficaro EP, Wieland DM, Koeppe RA. In vivo mapping of cholinergic terminals in normal aging, Alzheimer's disease, and Parkinson's disease. Annals of neurology. 1996; 40:399–410. [PubMed: 8797529]

Larsen AK, Brennum LT, Egebjerg J, Sanchez C, Halldin C, Andersen PH. Selectivity of ^{3}H-MADAM binding to 5-hydroxytryptamine transporters in vitro and in vivo in mice: Correlation with behavioural effects. British journal of pharmacology. 2004; 141:1015–1023. [PubMed: 14993096]

Lester DB, Rogers TD, Blaha CD. Acetylcholine-dopamine interactions in the pathophysiology and treatment of CNS disorders. CNS neuroscience & therapeutics. 2010; 16:137–162. [PubMed: 20370804]

Li J, Zhang X, Zhang Z, Padakanti PK, Jin H, Cui J, Li A, Zeng D, Rath NP, Flores H, Perlmutter JS, Parsons SM, Tu Z. Heteroaromatic and aniline derivatives of piperidines as potent ligands for vesicular acetylcholine transporter. Journal of medicinal chemistry. 2013; 56:6216–6233. [PubMed: 23802889]

Mulholland GK, Wieland DM, Kilbourn MR, Frey KA, Sherman PS, Carey JE, Kuhl DE. [^{18}F]Fluoroethoxy-benzovesamicol, a PET radiotracer for the vesicular acetylcholine transporter and cholinergic synapses. Synapse (New York, NY). 1998; 30:263–274.

Nagren K, Halldin C, Rinne JO. Radiopharmaceuticals for positron emission tomography investigations of Alzheimer's disease. European journal of nuclear medicine and molecular imaging. 2010; 37:1575–1593. [PubMed: 20033156]

Parent MJ, Bedard MA, Aliaga A, Minuzzi L, Mechawar N, Soucy JP, Schirrmacher E, Kostikov A, Gauthier SG, Rosa-Neto P. Cholinergic depletion in Alzheimer's disease shown by [^{18}F]FEOBV autoradiography. International journal of molecular imaging. 2013; 2013 205045.

Pavese N. PET studies in Parkinson's disease motor and cognitive dysfunction. Parkinsonism & related disorders. 2012; 18(Suppl 1):S96–99. [PubMed: 22166468]

Petrou M, Frey KA, Kilbourn MR, Scott PJ, Raffel DM, Bohnen NI, Muller ML, Albin RL, Koeppe RA. In vivo imaging of human cholinergic nerve terminals with (-)-5-^{18}F-fluoroethoxybenzovesamicol: Biodistribution, dosimetry, and tracer kinetic analyses. Journal of nuclear medicine : official publication, Society of Nuclear Medicine. 2014; 55:396–404.

Pettersen EF, Goddard TD, Huang CC, Couch GS, Greenblatt DM, Meng EC, Ferrin TE. UCSF Chimera - A visualization system for exploratory research and analysis. Journal of computational chemistry. 2004; 25:1605–1612. [PubMed: 15264254]

Pirker W, Holler I, Gerschlager W, Asenbaum S, Zettinig G, Brucke T. Measuring the rate of progression of Parkinson's disease over a 5-year period with p-CIT SPECT. Movement disorders : official journal of the Movement Disorder Society. 2003; 18:1266–1272. [PubMed: 14639666]

Radestock S, Forrest LR. The alternating-access mechanism of MFS transporters arises from inverted-topology repeats. Journal of molecular biology. 2011; 407:698–715. [PubMed: 21315728]

Ritchie DW, Venkatraman V. Ultra-fast FFT protein docking on graphics processors. Bioinformatics (Oxford, England). 2010; 26:2398–2405.

Ruberg M, Rieger F, Villageois A, Bonnet AM, Agid Y. Acetylcholinesterase and butyrylcholinesterase in frontal cortex and cerebrospinal fluid of demented and non-demented patients with Parkinson's disease. Brain research. 1986; 362:83–91. [PubMed: 3942870]

Schliebs R, Arendt T. The cholinergic system in aging and neuronal degeneration. Behavioural brain research. 2011; 221:555–563. [PubMed: 21145918]

Seibyl JP, Marek KL, Quinlan D, Sheff K, Zoghbi S, Zea-Ponce Y, Baldwin RM, Fussell B, Smith EO, Charney DS, van Dyck CH, Hoffer PB, Innis RB. Decreased single-photon emission

computed tomographic [^{123}I] p-CIT striatal uptake correlates with symptom severity in Parkinson's disease. Annals of neurology. 1995; 38:589–598. [PubMed: 7574455]

Shimada H, Hirano S, Shinotoh H, Aotsuka A, Sato K, Tanaka N, Ota T, Asahina M, Fukushi K, Kuwabara S, Hattori T, Suhara T, Irie T. Mapping of brain acetylcholinesterase alterations in Lewy body disease by PET. Neurology. 2009; 73:273–278. [PubMed: 19474411]

Steinfels GF, Alberici GP, Tam SW, Cook L. Biochemical, behavioral, and electrophysiologic actions of the selective sigma receptor ligand (+)-pentazocine. Neuropsychopharmacology : official publication of the American College of Neuropsychopharmacology. 1988; 1:321–327. [PubMed: 2855202]

Tu Z, Efange SM, Xu J, Li S, Jones LA, Parsons SM, Mach RH. Synthesis and in vitro and in vivo evaluation of ^{18}F-labeled positron emission tomography (PET) ligands for imaging the vesicular acetylcholine transporter. Journal of medicinal chemistry. 2009; 52:1358–1369. [PubMed: 19203271]

Tu Z, Wang W, Cui J, Zhang X, Lu X, Xu J, Parsons SM. Synthesis and evaluation of in vitro bioactivity for vesicular acetylcholine transporter inhibitors containing two carbonyl groups. Bioorganic & medicinal chemistry. 2012; 20:4422–4429. [PubMed: 22739089]

Tu Z, Xu J, Jones LA, Li S, Dumstorff C, Vangveravong S, Chen DL, Wheeler KT, Welch MJ, Mach RH. Fluorine-18-labeled benzamide analogues for imaging the sigma2 receptor status of solid tumors with positron emission tomography. Journal of medicinal chemistry. 2007; 50:3194–3204. [PubMed: 17579383]

Verhoest PR, Chapin DS, Corman M, Fonseca K, Harms JF, Hou X, Marr ES, Menniti FS, Nelson F, O'Connor R, Pandit J, Proulx-Lafrance C, Schmidt AW, Schmidt CJ, Suiciak JA, Liras S. Discovery of a novel class of phosphodiesterase 10A inhibitors and identification of clinical candidate 2-[4-(1-methyl-4-pyridin-4-yl-1H-pyrazol-3-yl)-phenoxymethyl]-quinoline (PF-2545920) for the treatment of schizophrenia. Journal of medicinal chemistry. 2009; 52:5188–5196. [PubMed: 19630403]

Weihe E, Tao-Cheng JH, Schafer MK, Erickson JD, Eiden LE. Visualization of the vesicular acetylcholine transporter in cholinergic nerve terminals and its targeting to a specific population of small synaptic vesicles. Proceedings of the National Academy of Sciences of the United States of America. 1996; 93:3547–3552. [PubMed: 8622973]

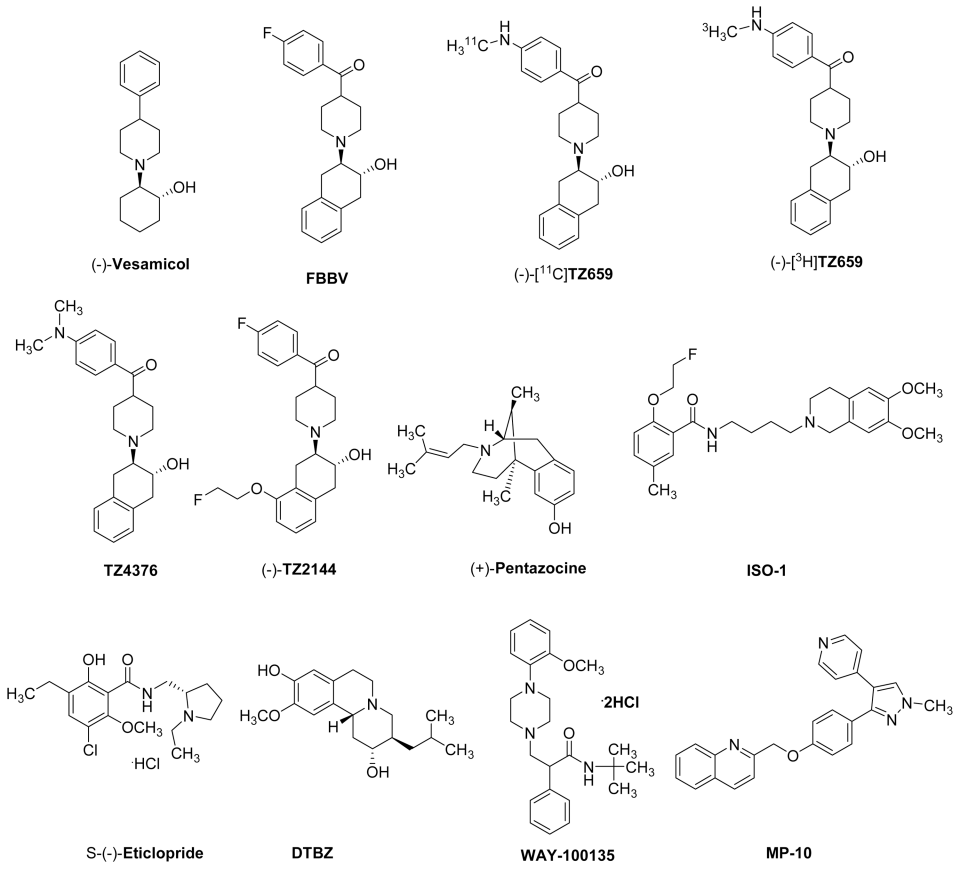

Fig. 1.

Chemical structures of (-)-[^{11}C]**TZ659**, (-)-[^{3}H]**TZ659** and other compounds used in the competitive binding assay.

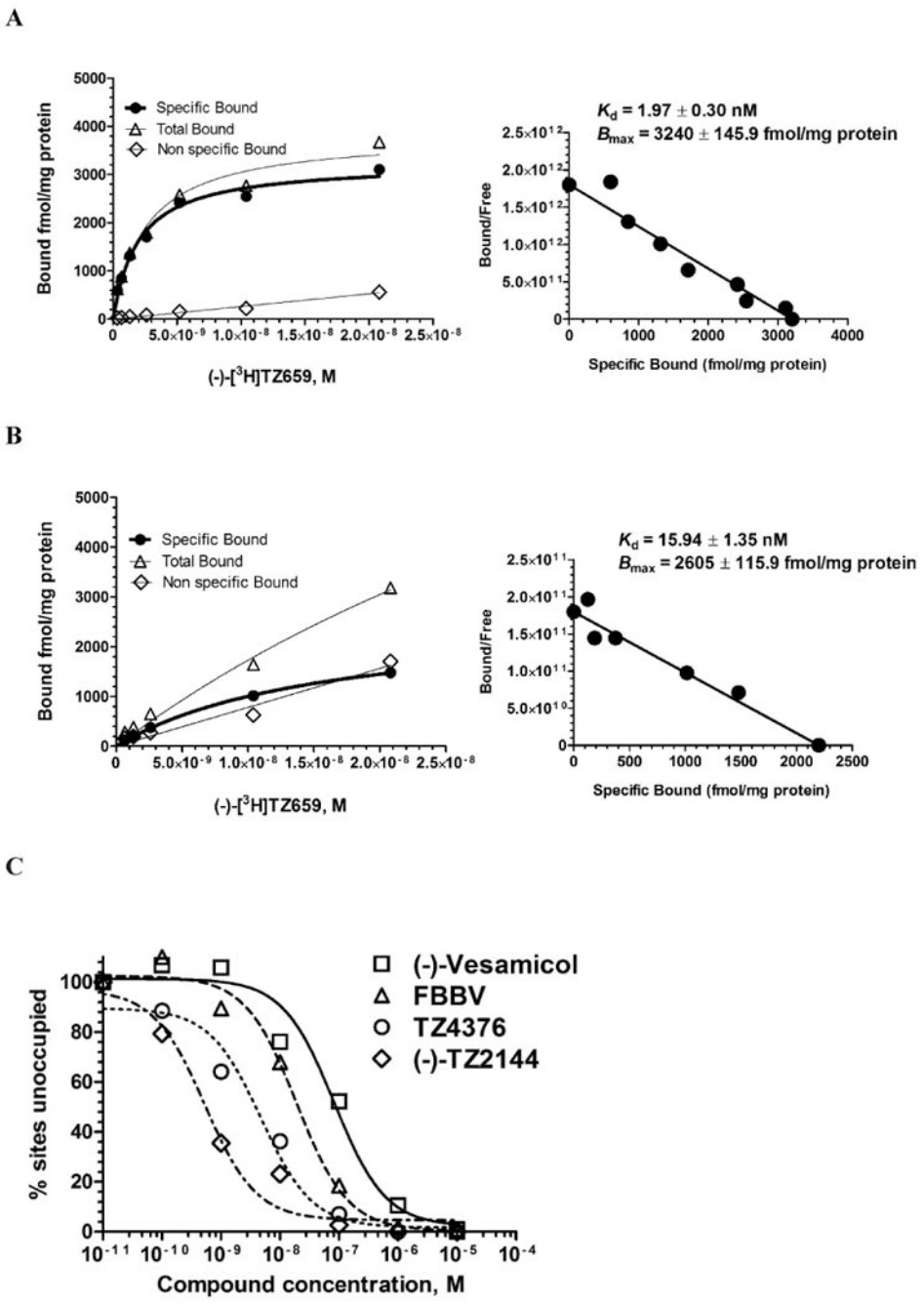

Fig. 2.

Saturation and competitive binding analysis of (-)-[^{3}H]**TZ659** to VAChT in homogenates of PC12$^{A123.7}$ cells Representative saturation binding analysis using PC12$^{A123.7}$ cells transfected with wild type hVAChT **(A)** and PC12$^{A123.7}$ cells transfected with mutant W331A hVAChT **(B)**. Representative competitive binding analysis using PC12$^{A123.7}$ cells transfected with wild type hVAChT **(C)**. The K_i values were shown in Table 1.

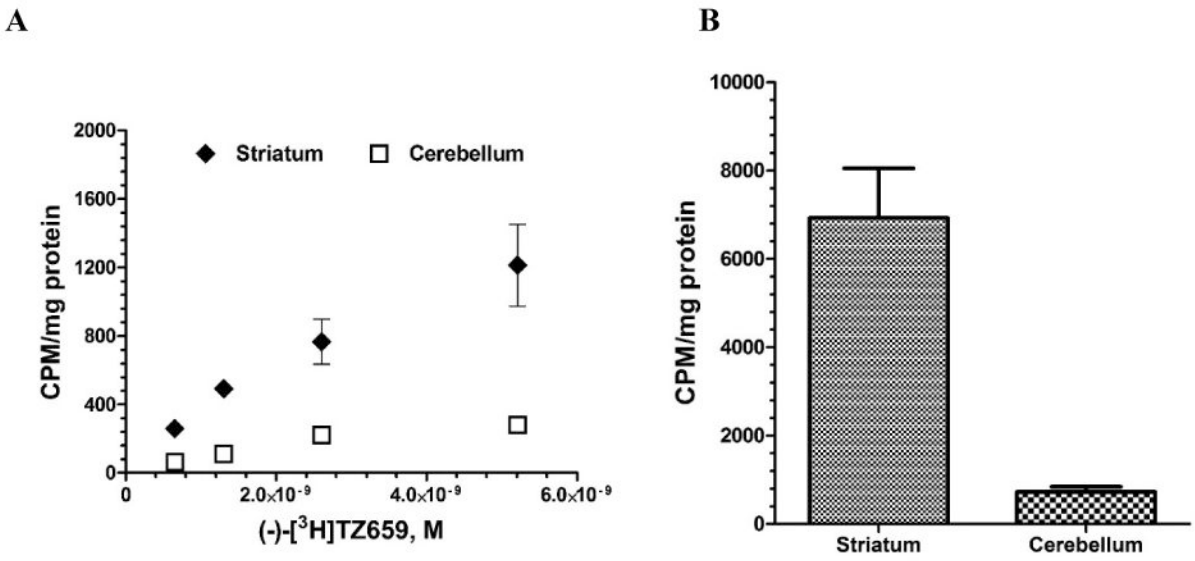

Fig. 3.

In vitro and *ex vivo* assays of radiolabeled (-)-**TZ659** to rat brain homogenates. **(A)** *In vitro* binding assay of (-)-[^{3}H]**TZ659** to rat brain homogenates. Homogenates of striatum and cerebellum were incubated with different concentrations of radioligand for 60 min. Subsequently, the radioactivity was measured and expressed graph as counts per minute per mg protein (CPM/mg protein). **(B)** *Ex vivo* uptake of (-)-[^{11}C]**TZ659** in rat striatum and cerebellum filtered homogenates. Rats were injected i.v. (n = 4) and the radiotracer uptake was measured after 60 min. The uptake in filtered homogenates was expressed as CPM/mg protein.

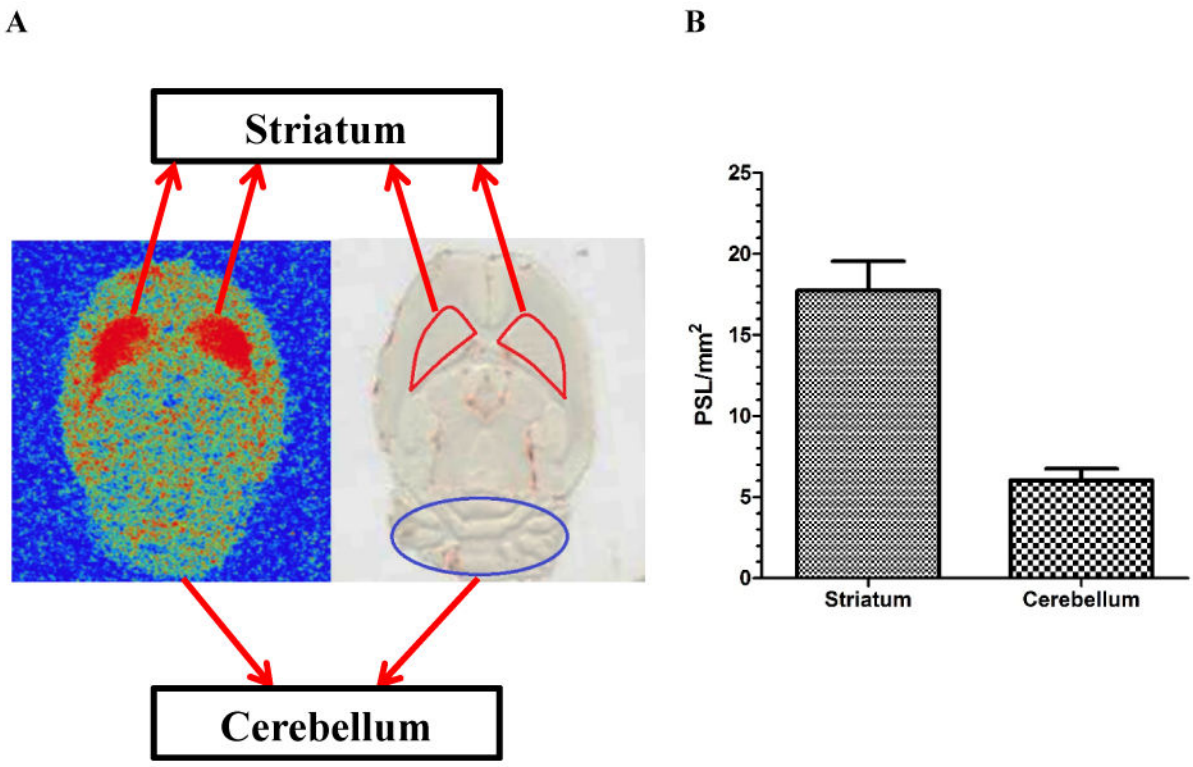

Fig. 4.

Ex vivo autoradiography of (-)-[^{11}C]**TZ659** in rat brain. **(A)** Horizontal sections showed strong binding of (-)-[^{11}C]**TZ659** in striatum and low binding in cerebellum. **(B)** Bars represent binding intensity (photo-stimulated luminescence signals per square millimeter, PSL/mm^2) of (-)-[^{11}C]**TZ659** after background subtraction.

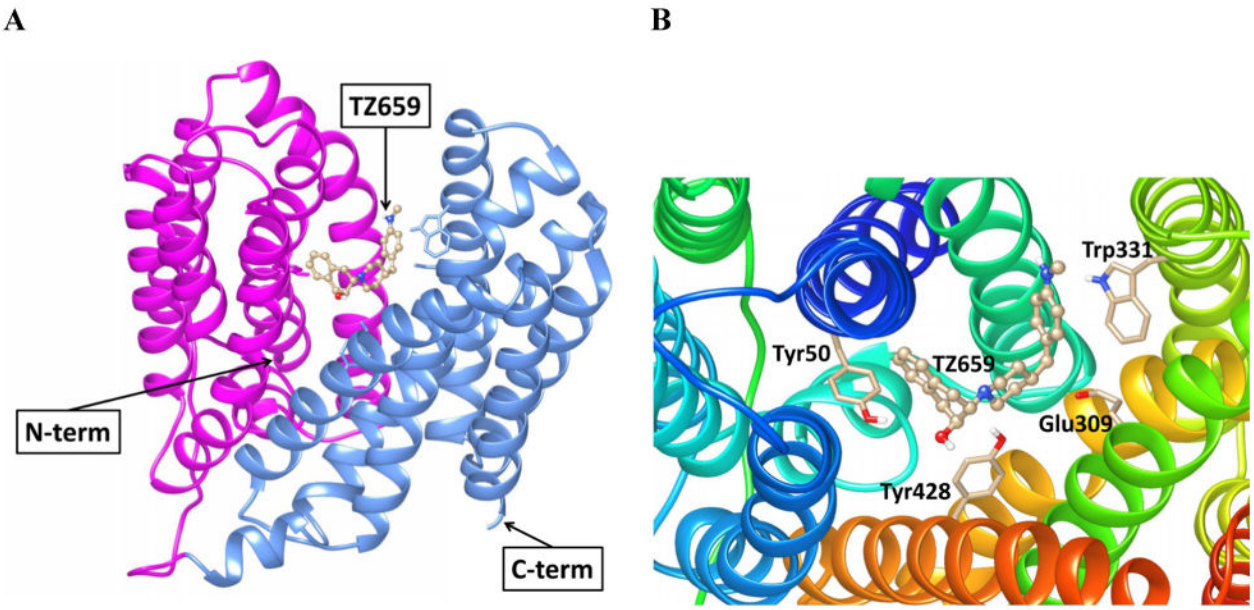

Fig. 5.

Homology modeling structure complex of (-)-**TZ659** to hVAChT. **(A)** The 12-span transmembrane (TM) domain of hVAChT is modeled with crystal structure of major facilitator superfamily (MFS) glycerol-3-phosphate transport. Modeling structure of hVAChT is shown with N-terminal 6-helex bundle in magenta, C-terminal 6-helix bundle in blue, and (-)-**TZ659** as a ball and stick model. Both N-terminal TM and C-terminal TM end to the vesicle lumen. (-)-**TZ659** specifically binds to the hinge region of N-terminal 6-helex bundle and C-terminal 6-helix bundle. **(B)** Close-up molecular interface shows a ball and stick of (-)-**TZ659** fits to the binding pocket (near Tyr50, Glu309, Trp331 and Tyr 428) of the conserved transporter of MFS.

Table 1

Summary of the VAChT binding affinity for CNS ligands obtained from competitive binding study with (-)-[^{3}H]**TZ659** using homogenates of hVAChT transfected PC12$^{A123.7}$ cells.

Compounds	K_i, nM	Notes
(-)-**TZ2144**	0.20 ± 0.03	VAChT ligand
TZ4376	1.82 ± 0.23	VAChT ligand
FBBV	7.17 ± 0.66	VAChT ligand
(-)-Vesamicol	31.35 ± 5.17	VAChT and σ_1 receptor ligand
(+)-Pentazocine	>1000	σ_1 receptor ligand
ISO-1	>1000	σ_2 receptor ligand
S-(-)-**Eticlopride**	>1000	D_2 receptor ligand
DTBZ	>1000	VMAT2 ligand
WAY-100135	>1000	5-HT_{1A} receptor ligand
MP-10	>1000	PDE10A ligand